Article:
Yu, L, Song, M, Williams, PT orcid.org/0000-0003-0401-9326 et al. (1 more author) (2019) Alumina-Supported Spinel $NiAl_2O_4$ as a Catalyst for Re-forming Pyrolysis Gas. Industrial and Engineering Chemistry Research, 58 (27). pp. 11770-11778. ISSN 0888-5885

https://doi.org/10.1021/acs.iecr.9b01006

Alumina-supported spinel $NiAl_2O_4$ as a catalyst for reforming pyrolysis gas

Lei Yu[1], Min Song[1*], Paul T. Williams[2], Yuexing Wei[1]

[1]Ministry of Education of Key Laboratory of Energy Thermal Conversion and Control, School of Energy and Environment, Southeast University, Nanjing, 210096, China

[2]School of Chemical & Process Engineering, University of Leeds, LS2 9JT, UK

*Correspondence author: Phone: +86-13770606581. Fax: +86-025-83790986. Email: minsong@seu.edu.cn

ORCID: Min Song: 0000-0002-0002-0568

Abstract:

A spinel structure for $NiAl_2O_4$ in nickel-based alumina has a significant impact on catalytic performance. To illustrate the relationship between the textural properties of spinel and catalytic performance, four nickel-based alumina catalysts using co-precipitation with different calcination temperatures were prepared and evaluated for the reforming of simulated pyrolysis gas (CH_4+CO_2) then applied to the reforming of gaseous products from rice husks pyrolysis. The results indicated that the spinel structure could improve the catalytic performance. Various characterization methods combined with mechanism analysis were applied to illustrate the contribution of surface properties and structure parameters of the spinel catalysts on catalytic performance. The influence of spinel structure in catalysts on the textural properties, the specific form of surface nickel species and the anti-coking ability of the catalysts have been established. Finally, the relationship between the spinel structure of the catalysts and the catalytic reforming performance has been thoroughly explained.

Keywords: Spinel structure, Nickel-based alumina, Catalytic performance, Biomass, Pyrolysis-reforming.

1. Introduction

Currently, production methods of the syngas (H_2 and CO) generation have attracted much attention. At present, industrial production of syngas is mostly from the conversion of fossil fuels [1], such as coal gasification [2, 3], methane reforming [4] and partial oxidation of methane [5, 6], etc. However, in consideration of the non-renewable nature of fossil fuels and the environmental impact caused by greenhouse gases, it is a global interest to find renewable and clean energy sources as alternatives to fossil fuels. Abundant worldwide biomass can be obtained from various cheap and non-food resources [7, 8], such as energy crops, agricultural residues, organic wastes, etc. Therefore, thermochemical conversion technology for biomass [9, 10] e.g. gasification and pyrolysis, has been considered as a sustainable method for syngas production because of the inexpensive and renewable nature of the raw material. Among various biomass thermochemical conversion technologies, a two-stage pyrolysis-reforming system [11] has been used to convert biomass to syngas, which possesses unique advantages. The biomass is first rapidly pyrolyzed in the first stage, and the derived vapors, excluding the biochar (retained in the first stage), is catalytically reformed in the second stage. The biomass is not mixed with the catalyst, which can significantly reduce the carbon deposition on the catalyst surface and improve its reforming performance.

A stable and efficient catalyst has a significant impact on gasification and pyrolysis [12, 13]. Among various catalysts, nickel-based catalysts supported on alumina have been typically used because of the high catalytic performance and low cost. Much research has focused on the modification of nickel-based alumina [14] through the cooperation of transition metal [15], alkaline earth metal [16] and alkali metal [17] in order to achieve stable catalysts which can resist coking and sintering effectively. Some research has suggested that the presence of spinel structure in nickel-based alumina catalysts has an important influence on the catalytic performance.

Initially, the spinel structure was proposed in nickel-based alumina catalysts used in methane reforming. A series of mixed oxides close to $NiAl_2O_4$ were reported using a sol-gel method [18] and the optimum preparation process was also obtained. The effect of $NiAl_2O_4$ on Ni/Al_2O_3 stability [19] was also illustrated during the dry reforming of methane. In addition, the $NiAl_2O_4$ catalyst was reported for [20] syngas production via dry reforming of methane and the physical-chemical properties of the catalyst was discussed. Some researches [21, 22] also prepared the catalysts derived from $NiAl_2O_4$ using different methods and applied them into oxidative steam reforming and steam reforming of methane. It was demonstrated that a spinel $NiAl_2O_4$ catalyst is a more efficient catalyst with various chemical nature compared with commercial catalyst. Also, the spinel $NiAl_2O_4$ structure was identified that played an important role in the catalytic performance of $Ni/CaAlO_X$ catalysts [23] used for pyrolysis-steam reforming of biomass. However, the structural characteristics of spinel contain many aspects. Which one is essential for determining the catalytic performance? The relationship between the spinel structure and catalytic performance has not been clearly explored. Therefore, it is necessary to illustrate what causes the spinel structure to improve the catalytic performance of nickel-based alumina.

The effect of the spinel structure on the catalytic performance of nickel-based alumina has now been thoroughly investigated in this study. Four nickel-based alumina catalysts were prepared using the co-precipitation method and calcined at different temperatures. The catalytic performance of obtained spinel catalysts was investigated for the reforming of simulated pyrolysis gas (CH_4+CO_2) then applied to the reforming of gaseous products from rice husks pyrolysis. In addition, various characterization methods were applied to illustrate the textural properties and surface characteristic parameters of catalysts so as to reveal the nature of the influence of spinel structure on the catalytic performance of biomass thermochemical conversion.

2. Materials and methods

2.1 Catalyst preparation

The co-precipitation method was applied to prepare the spinel $NiAl_2O_4$ catalysts. The analytically pure nickel nitrate ($Ni(NO_3)_2 \cdot 6H_2O$), aluminum nitrate ($Al(NO_3)_3 \cdot 9H_2O$) and sodium carbonate (Na_2CO_3) were used as the precipitation precursors. The total mass content of nickel was 5% [24]. The mixed solution of nickel nitrate and aluminum nitrate was co-precipitated with the solution of sodium carbonate using two peristaltic pumps in a beaker placed in magnetic stirrer at 40 °C. After co-precipitation, the suspension was aged for 30 min to make the grain grow, then the precipitant was collected by filtration, washed to neutral and dried at 105 °C. The dried product was calcined for 120 min at 300 °C, 500 °C, 700 °C, and 900 °C under nitrogen atmosphere, respectively. The four fresh catalysts obtained were denoted as NA-300, NA-500, NA-700, and NA-900 respectively. The detailed preparation conditions can be found in Table S1.

2.2 Evaluation of catalytic performance

The main gas components of biomass pyrolysis are CH_4, CO_2, CO, H_2O, H_2, etc. The reforming of gaseous products from biomass pyrolysis can be considered as mixed reforming including dry reforming and steam reforming of hydrocarbon. Dry reforming is one of the key reactions which could lead to carbon deposition of catalyst. Therefore, we selected the components of CH_4 and CO_2 to serve as the simplified simulated pyrolysis gaseous products to evaluate the performance of spinel structure catalysts. The prepared catalysts were then applied into the real pyrolysis-reforming system to reveal the catalytic reforming performance of gaseous products from rice husks pyrolysis.

2.2.1 Catalytic reforming of simulated pyrolysis gas

Firstly, the catalysts were applied to the reforming of simulated pyrolysis gas using a fixed bed reactor [24]

shown in Figure S1 (A). 0.25 g catalyst between 40 and 60 meshes was loaded into a stainless steel tube of 8mm in diameter. Before reforming, the catalysts were reduced in a pure hydrogen atmosphere with a flow rate of 50 mL/min at the specific temperature based on the results of H_2 temperature programmed reduction. The reduction was kept for 2 h and then flushed under a N_2 flow of 50 mL/min. The N_2 served as a carrier gas to maintain atmospheric pressure and kept the total flow constant. The gas composition was analyzed by a Gas chromatograph (GC5890, Kejie, China) equipped with TCD and FID detectors and capillary column [25].

To evaluate the catalytic performance, some parameters are defined. The CH_4 conversion ratio is defined as follows:

$$\chi_{CH_4} = \frac{F_{in,\ CH_4} - F_{out,\ CH_4}}{F_{in,\ CH_4}} \quad (1)$$

Where F_{in,CH_4} is the CH_4 flow rate in input gas, and F_{out,CH_4} is the CH_4 flow rate in products.

The CO_2 conversion ratio is defined as follows:

$$\chi_{CO_2} = \frac{F_{in,CO_2} - F_{out,CO_2}}{F_{in,CO_2}} \quad (2)$$

Where F_{in,CO_2} is the CO_2 flow rate in input gas, and F_{out,CO_2} is the CO_2 flow rate in products.

The H_2 selectivity is defined as follows:

$$\chi_{H_2} = \frac{F_{out,H_2}}{(F_{in,CH_4} - F_{out,CH_4})*2} \quad (3)$$

Where F_{out,H_2} is the H_2 flow rate in products.

2.2.2 Real pyrolysis-reforming of biomass

The four as-prepared catalysts were then applied to the reforming of gaseous products from rice husks pyrolysis to illustrate the catalytic performance. A two-stage reactor in Figure S1 (B) was used in this work. In the first stage reactor, the rice husks were decomposed into pyrolysis vapors, then passed to the second stage for catalytic steam reforming. The catalyst was loaded in the second stage. For each experiment, N_2

served as the carrier gas with a flow rate of 100 mL/min. 1 g of rice husks and 0.25 g fresh catalyst were loaded in the first and second stage respectively. The second stage was firstly heated to 800 °C until the temperature was stabilized. Then the first stage, pyrolysis section, was heated to 600 °C at a heating rate of 40 °C/min. When the first stage started to be heated, the water would be injected to the second stage using a syringe pump with a flow rate of 4 mL/h so as to produce steam as the reforming agent. The total reaction time for each experiment was about 40 min.

The liquid products were collected by two condensers, which were air cooled and dry-ice cooled, respectively. The uncondensed gases were collected by a 25 L gas sample bag then analyzed by two off-line gas chromatographs reported in our previous work [26]. It is noted that the oil product was not evaluated in this work because hydrogen-enriched gas was the target product. The gas, char residue yield and mass balance were calculated via Eq. (3) - (5), respectively.

$$\text{Gas yield (wt \%)} = \frac{\text{weight of gas}}{\text{weight of biomass sample}} * 100\% \quad (4)$$

$$\text{Char residue yield (wt \%)} = \frac{\text{weight of char residue}}{\text{weight of biomass sample}} * 100\% \quad (5)$$

$$\text{Mass balance (wt \%)} = \frac{\text{weight of gas, char residue, and liquid}}{\text{weight of biomass sample + weight of injected water}} * 100\% \quad (6)$$

2.3 Characterization of catalysts

Various characterization methods were applied to investigate the surface properties of the catalysts. The H_2-temperature programmed reduction (H_2-TPR) (FineSorb3010, Finetec, China) was applied to investigate the surface nickel species of catalysts, the reducibility of fresh catalysts and the interaction between active metal and support. The X-ray diffraction (XRD) (Smart lab 3, Rigaku, Japan) was used to illustrate the crystallite size and crystal structure of fresh catalysts. The surface structure parameters and N_2 adsorption-desorption isotherms of different catalysts were obtained by a specific surface area and pore size analyzer (V-

Sorb 2800P, Gold APP, China). The coke deposited on catalysts surface for reforming of simulated pyrolysis gas was characterized by O_2-temperature programmed oxidation (O_2-TPO) conducted under 5% O_2 atmosphere (FineSorb3010, Finetec, China). Catalysts were also analyzed using transmission electron microscopy (TEM) (Tecnai G2 F20, FEI, USA) to obtain the detailed morphology of fresh catalysts.

3. Results and discussion

3.1 Characterization of the fresh catalysts

3.1.1 Surface morphology analysis of fresh catalysts

Firstly, the detailed morphology of four fresh catalysts was illustrated by TEM under the resolution of 2 nm and 50 nm as shown in Figure 1. From the images under 50 nm resolution, the morphology of the catalysts has obvious changes from 300 °C to 900 °C. It can be observed the particle size of catalyst NA-300 calcined at 300 °C is larger than that of the catalyst NA-900 prepared at 900 °C. Zooming to 2 nm resolution, based on the enlargement of local region shown in the images, the prismatic structure of spinel could be observed in catalyst NA-900, NA-700 and NA-500, but except NA-300. The crystal plane spacing of spinel on the surface of three catalysts is about 0.260 nm, which is close to the crystal plane (220) [27] of spinel. And the formation of the lattice of spinel oxide was confirmed by X-ray diffraction and H_2-TPR results below.

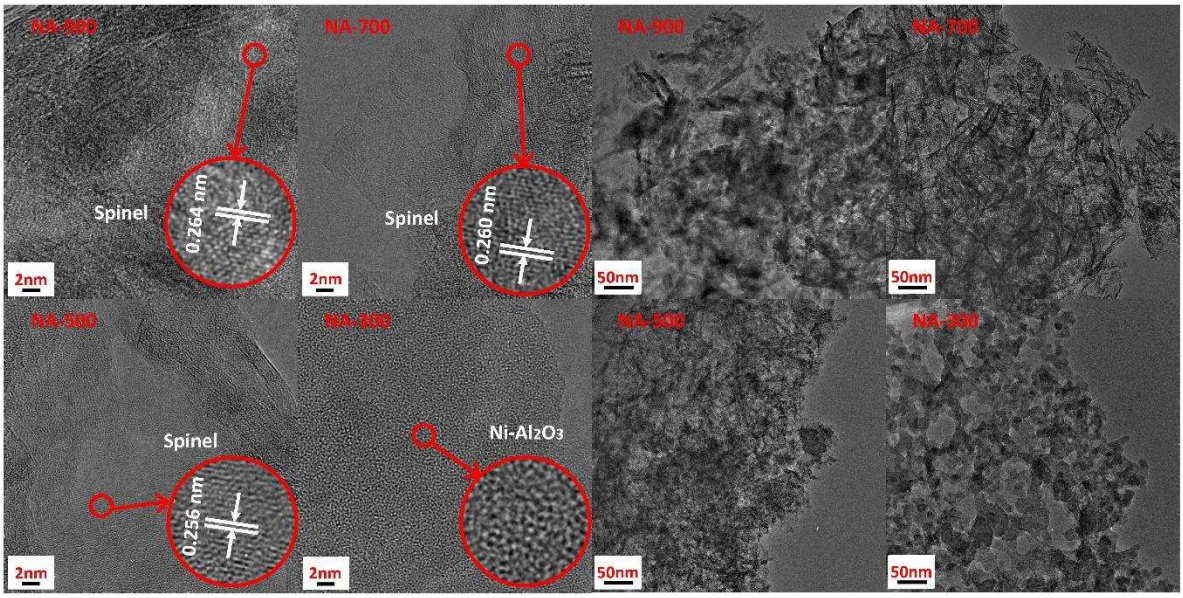

Figure 1 TEM images of four fresh catalysts

3.1.2 Crystallite structure analysis of fresh catalysts

To verify the spinel structure on catalysts, the four fresh catalysts before reduction were characterized by XRD to validate the formation of the lattice of spinel oxide and the crystal size was also calculated based on Scherrer equation. Since the catalysts were not yet reduced, nickel exists in the form of nickel oxide in the catalysts. As can be seen from the XRD patterns in Figure 2, the surface crystal structure is various for four catalysts with different calcination temperatures. For the catalyst NA-300, there are only NiO phase (2θ = 37.2°, 44.5°, and 63°) and Al_2O_3 phase (2θ = 37.2°, 46°, and 66.7°) [26, 11] on the catalyst surface, while the spinel structure $NiAl_2O_4$ is not detected. And the peak at 37.2° is the combination of NiO and Al_2O_3 phases. When the calcination temperature was increased, the phase of spinel $NiAl_2O_4$ could be observed on the XRD patterns of other catalysts. For the catalyst NA-500, the characteristic peaks of spinel can be observed in the vicinity of 19.9°, 30°, 37.2°, and 60.5°. However, the peaks of Al_2O_3 and NiO also can be observed at 46° and 63° respectively in addition to the coincidence positions with spinel. This indicates that there is a coexistence of nickel oxide phase, alumina phase and spinel phase in the catalyst NA-500. While for the catalyst NA-700

and NA-900, separate peaks of Al_2O_3 and NiO cannot be observed. The existence of $NiAl_2O_4$ phase could be evidenced by the diffraction peak at 19.9°, 30°, 37.2°, 46°, 60.5° and 66.5° [26]. Some characteristic peaks of spinel cover the peak positions of Al_2O_3 and NiO. It can be considered that the nickel oxide component mainly exists in the form of spinel structure in these two catalysts.

In order to illustrate the effect of spinel structure on the crystal size of nickel species, two XRD peak positions near 37.2° and 46° were selected to calculate the crystallite size as presented in Table 1. It can be found that the crystal size of nickel species in the form of spinel is smaller than that in the form of NiO which is not combined with Al_2O_3. The higher the calcination temperature, the smaller the crystal size of the spinel structure catalyst. The smaller crystal size could contribute to anti-coking of the catalysts [28].

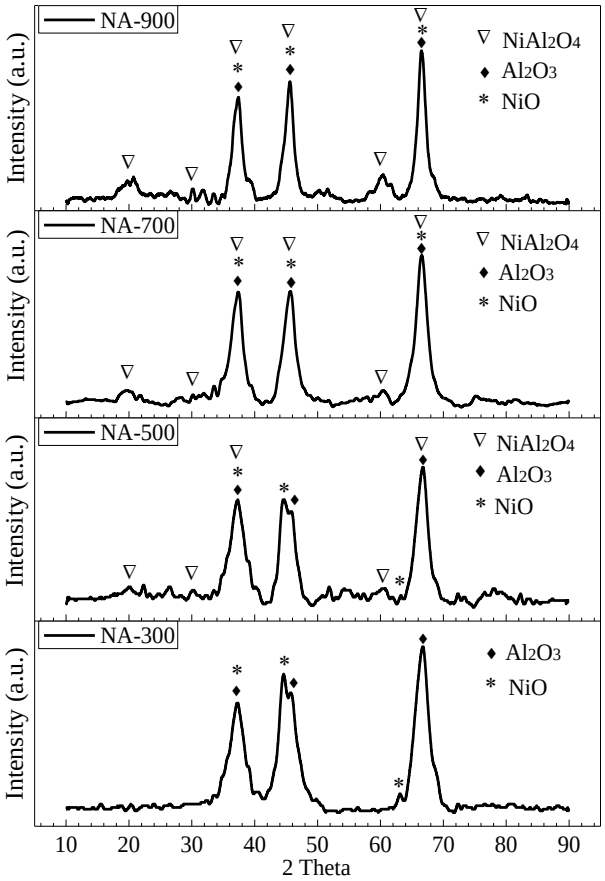

Figure 2 XRD analysis of fresh catalysts ($NiAl_2O_4$: #78-1601, NiO: #44-1159, Al_2O_3: #10-0425)

Table 1 Particle size of spinel $NiAl_2O_4$ in catalysts

2-Theta(°)	Crystal Size(nm)			
	NA-300	NA-500	NA-700	NA-900
37.2	11.57	11.50	9.93	7.59
46	8.72	8.33	7.74	7.23

3.1.3 Nickel species analysis on catalysts surface

The spinel structure in catalyst has a significant impact on the nickel species on the catalyst surface. To identify the nickel species presented in each sample and their reducibility, the analysis of the four synthesized catalysts by H_2-TPR was performed. The results are presented in Figure 3. In some researches [19], the nickel species were divided into three types depending on the different reduction temperature, the free NiO, the "surface $NiAl_2O_4$", and the crystalline spinel $NiAl_2O_4$. Another researches [21, 22] also reported the same phenomenon in nickel-based alumina and named the reducible Ni^{2+} species with α, β, and γ. However, it should be noticed that there is also a reduction peak of nickel species in their results when the temperature is less than 300℃, which they both neglected. So we make a change to the way the nickel species divided. The nickel species in the prepared catalysts could be divided into four types in Figure 3, whereas the NiO species with a reduction temperature below 350 °C corresponded to the free NiO, the NiO-Al_2O_3 species with a reduction temperature at 350-600 °C corresponded to the NiO just supported on Al_2O_3, the bulk $NiAl_2O_4$ species with reducibility at moderate temperatures (600-750 °C) were identified as Ni^{2+} ions that are not completely integrated into the spinel, and the spinel $NiAl_2O_4$ species with a reduction temperature over 750 °C corresponded to the NiO in spinel structure. In addition, no reduction peaks of alumina support were observed in this reduction temperature range [21].

For the catalyst NA-300 calcined at 300 °C, it is observed three reduction peaks, which could be ascribed

to the free NiO species around 284 °C, the NiO-Al_2O_3 species around 441 °C and the bulk $NiAl_2O_4$ species with reducibility at 688 °C. The main nickel species are the NiO-Al_2O_3 and the bulk $NiAl_2O_4$ species. While for the catalyst NA-500 calcined over 500 °C, all four kinds of nickel species could be observed on the curves. The part of bulk $NiAl_2O_4$ species converted into the spinel structure with the increasing of calcination temperature. When the calcination temperature exceeds 700 °C, there is almost no nickel oxide of bulk $NiAl_2O_4$ species in the catalysts NA-700 and NA-900. The reduction peak shifts to higher temperature. The contrasted peak area also shows an increasing proportion of spinel structure, while other forms of nickel oxide species are becoming less. When the NiO converted from NiO-Al_2O_3 species to spinel species, the interaction between nickel and alumina will be enhanced, which could contribute to the resistance to catalyst sintering [28]. Combined with the results of TEM, XRD and H_2-TPR，it can be determined that the spinel structure of the catalyst can be formed at a calcination temperature above 500 °C. Most of the nickel species are presented in the form of a spinel structure with a calcination temperature over 700 °C. It is well known that the higher the reduction temperature of nickel species, the stronger the interaction between active metal and support, and the better the sintering resistance of the catalyst [28]. For nickel-based alumina catalysts, the spinel structure improves the interaction between active metal and support, which is conducive to the property of sintering resistance of the catalyst.

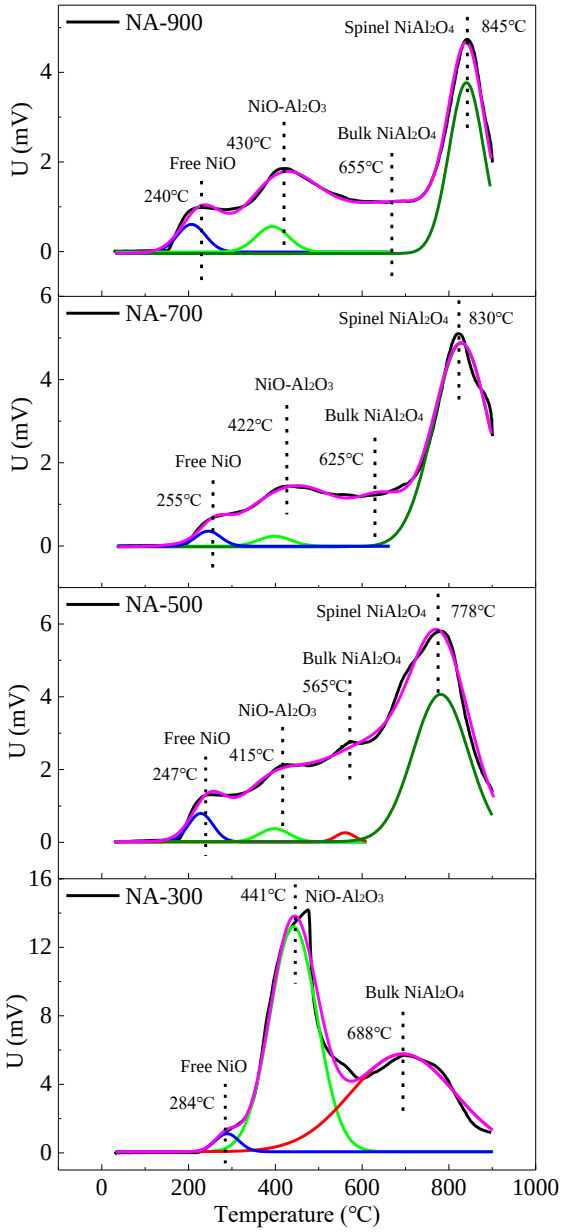

Figure 3 H_2-TPR of four fresh catalysts

3.1.4 Specific surface area and pore structure parameters

The catalytic reaction of heterogeneous catalysts is a process involving adsorption, surface reaction and desorption [29]. Therefore, the surface pore structure of the catalyst is closely related to the catalytic performance. The spinel $NiAl_2O_4$ also has an influence on the surface pore structure properties of the catalysts. To illustrate this impact, the specific surface area, pore structure parameters and N_2 adsorption-desorption isotherms of the

four fresh catalysts were determined by the Brunauer-Emmett-Teller (BET) method and the results are presented in Table 2 and Figure 4 respectively. Three kinds of surface areas and pore volumes as well as the average pore diameters were obtained. As shown in Table 2, the spinel structure can increase the surface pore size of catalyst and improve the micropore structure of catalyst surface. The catalyst NA-900 with more spinel structure has a larger micropore surface area and micropore volume. At the same time, the influence of calcination temperature on pore structure characteristics also shows a certain regularity. For the surface area, with the increasing of calcination temperature, the BET and mesopore-macropore surface area increase firstly then decrease. While for micropores, the value keeps increasing. Similarly, the total pore volume and mesopore-macropore pore volume also increase firstly then decrease, but the micropore pore volume continues increasing. In addition, the average pore diameters are increasing as the calcination temperature increases which is consistent with the results of pore size distribution shown in Figure 4. According to the results of pore size distribution in Figure 4, the surface of the catalyst is dominated by mesopores (2-50 nm). With the formation of spinel structure in the catalyst, the shape of N_2 adsorption-desorption isotherms gradually changes from Type IV (mesoporous material) for NA-300 to Type II (macroporous material) [30] for NA-900. To combined analyze the surface textural parameters with the catalytic performance of the catalysts in Figure 5 below, the catalytic performance of the prepared catalysts with a spinel structure will be better, which is consistent with the trend of pore size and microporous structural parameters. So it can be concluded that the spinel structure has a positive effect on the pore size and microporous structure parameters, which are also closely related to the catalytic performance of the catalyst.

Table 2 Specific surface area and Pore structure parameters of four fresh catalysts

Sample	S_{BET}(m²/g)	V_t (m³/g)	D_p (nm)	S_{BJH} (m²/g)	V_{BJH} (cm³/g)	$S_{T\text{-}plot}$ (m²/g)	$V_{t\text{-}Plot}$ (cm³/g)
NA-300	146.93	0.47	12.70	150.10	0.48	12.94	0.0043
NA-500	157.53	0.53	13.66	157.02	0.54	14.71	0.0051
NA-700	118.50	0.59	19.57	121.32	0.59	15.84	0.0061
NA-900	59.81	0.31	28.69	41.83	0.30	21.39	0.0095

S_{BET}: BET Specific surface area; V_t: Total Pore volume; D_p: Average pore diameter; S_{BJH}: Mesopore-macropore surface area; V_{BJH}: Mesopore-macropore Pore volume; $S_{T\text{-}plot}$: Micropore surface area; $V_{t\text{-}Plot}$: Micropore Pore volume;

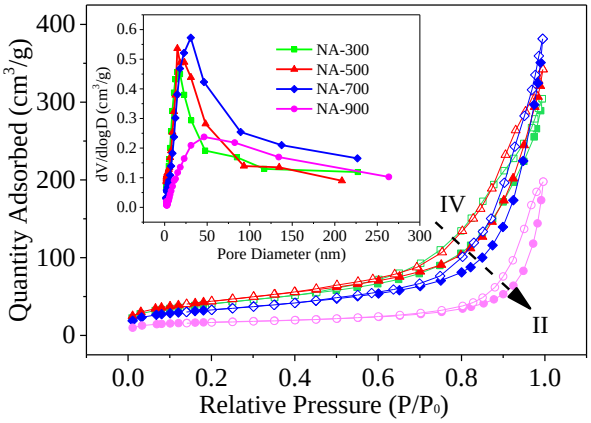

Figure 4 Pore size distribution and N_2 adsorption-desorption isotherms of the fresh catalysts (Solid: Adsorption; Open: Desorption)

3.2 Reforming of simulated pyrolysis gas (CH_4+CO_2)

3.2.1 Catalytic performance

To evaluate the catalytic performance of the catalysts with the spinel structure, the four catalysts were applied to the reforming of simulated pyrolysis gas (CH_4+CO_2). Before reforming the four catalysts were reduced at the temperature obtained from H_2-TPR results. The detailed reduction conditions of four catalysts are presented in Table S2. The catalytic performance of four catalysts at 650 °C and 750 °C is shown in Figure 5. Obviously, the results show that the catalysts with spinel structure calcined at relatively high temperature have a better catalytic performance in relation to CH_4 conversion in Figure5 (a), especially for the catalyst

NA-900. The catalyst with more spinel structure has better microporous properties and bigger pore size which could contribute to the adsorption and activation [31] of the raw feedstock gas. And the smaller crystallite size of the spinel catalysts can promote more feedstock gas to participate in the reforming. In addition, we can also analyze the reason why the catalyst NA-900 with spinel structure is superior to the conventional alumina supported catalyst NA-300 in terms of a molecular level and catalytic mechanism. Figure 6 (a) shows a three-dimensional structure of spinel $NiAl_2O_4$ catalyst. For the catalyst NA-300 without spinel structure, the atom oxygen surrounds the atom aluminum in the form of tetrahedron, the atom aluminum is tetrahedron coordination [32]. However, in the spinel structure catalyst NA-900, O surrounds Al in the form of octahedron [33], and Al is a stable octahedron coordination, which favors for anti-agglomerate at high temperature. When nickel oxide is reduced, there are two oxygen vacancies around nickel in the spinel structure, as shown in Figure 6 (b), while for the catalyst without spinel structure there are no oxygen vacancies after the reduction of nickel oxide. Based on the density functional theory (DFT) calculation results from Tao [27], the reaction mechanism of methane reforming with CO_2 on the catalyst surface can be shown in Figure 6 (c). Methane is firstly adsorbed on the catalyst surface and dissociates methyl functional groups and H atoms, while CO_2 dissociates oxygen atoms [34] after adsorption. For spinel structure catalysts, this oxygen will occupy the oxygen vacancy in the crystal structure. Subsequently, the methyl groups will combine with oxygen on the catalyst surface to form aldehyde functional groups, which continue to release H atoms. The oxygen comes from lattice oxygen of the support or oxygen dissociated from CO_2. Obviously, the oxygen dissociated from CO_2 occupying the oxygen vacancy is easier to combine with methyl than lattice oxygen, and the reduced spinel structure catalyst has exactly two oxygen vacancies. It's another reason why the catalytic performance of the spinel structure catalyst NA-900 is better than that of the catalyst NA-300 without spine structure.

For the ratio of H_2 to CO (H_2/CO) in Figure 5 (b), the influence of spinel is not obvious at 750 °C. The H_2/CO ratios of the four catalysts are close to 1. However, at 650 °C, the H_2/CO ratios of four catalysts have obvious changes. With the increasing of spinel proportion in the four catalysts, the ratio of H_2/CO increases. Compared with NA-300, the H_2/CO ratio of NA-900 is closer to 1. As we all know that dry reforming of methane serves as the main reaction in the reforming system, reverse water gas shift occurs as the side reaction [35]. At 650℃, the side reaction, reverse water gas shift, would consume the hydrogen and cause the H_2/CO ratio less than 1. However, because of the bigger pore size, developed microporous structure and smaller crystal size the catalysts with spinel structure can allow more feed gas to participate in the reforming reaction on the catalyst surface. At the same time, the unique crystal structure can promote more CO_2 to dissociate O atom, which could inhibit carbon deposition and promote the occurrence of the main reaction. In addition, for the selectivity of hydrogen in Figure 5 (c), in most cases, the selectivity of hydrogen is close to 1, which indicates that the hydrogen element from the methane involved in the reaction is converted mostly in the form of H_2. But for the catalyst NA-300 without spinel structure, the H_2 selectivity at relatively low temperature is below 1, which is ascribed that hydrogen is consumed by the reverse water gas shift reaction at low temperature.

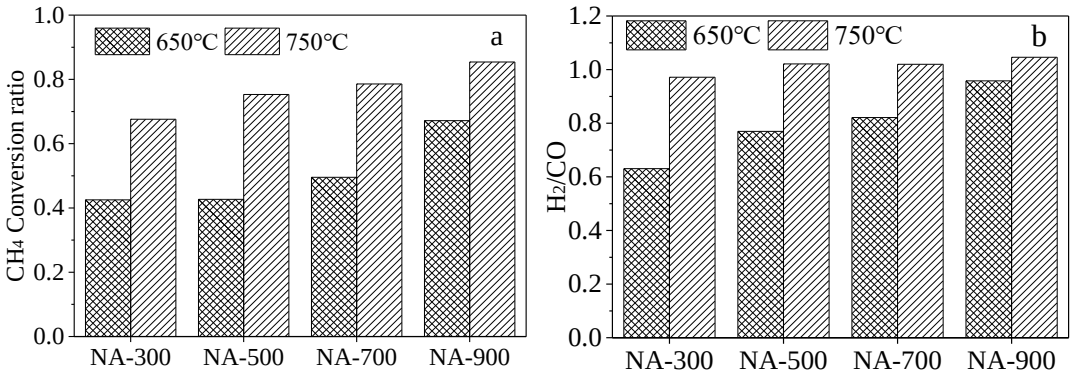

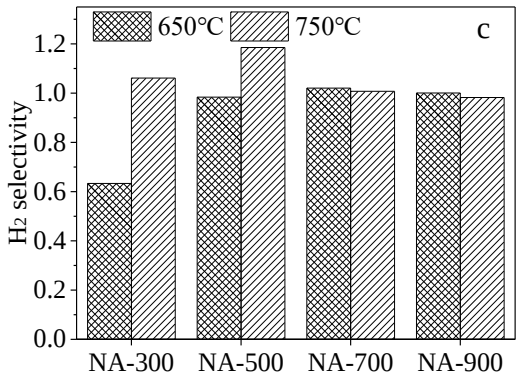

Figure 5 Catalytic performance of four catalysts reduced at the temperature of H_2-TPR results (a: CH_4 conversion ratio; b: ratio of H_2/CO; c: H_2 selectivity) (Catalyst dosage: 0.25 g, CO_2: 50mL/min, CH_4: 50 mL/min, N_2: 100 mL/min, GHSV: 48000 mL/min/g, Reforming Temperature: 650℃ and 750℃)

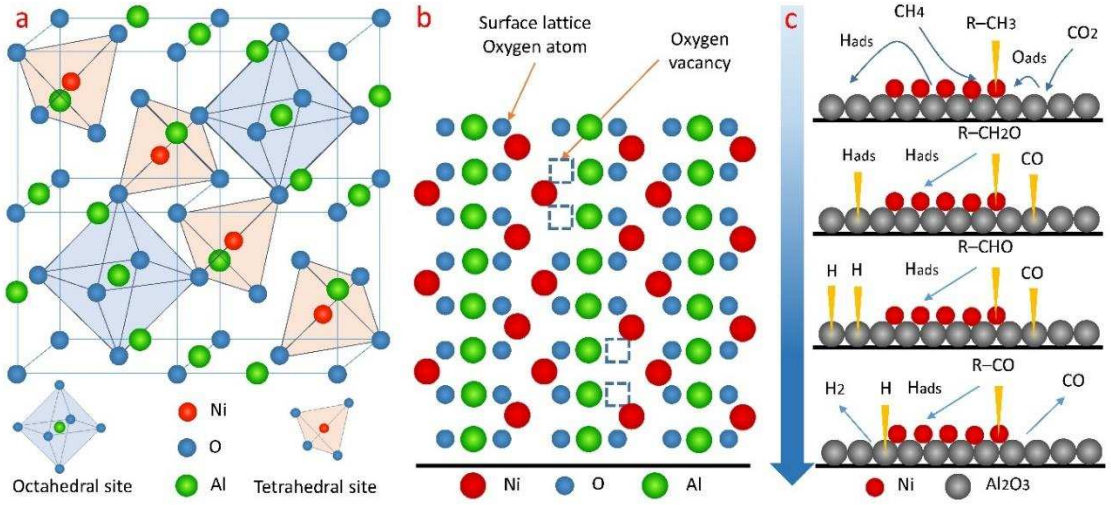

Figure 6 Schematic of the three-dimensional structure of spinel $NiAl_2O_4$ catalyst (a), Schematic of the surface of spinel $NiAl_2O_4$ catalyst (b) and reaction mechanism (c)

3.2.2 Surface coke analysis

In addition, the spinel structure also has an impact on the anti-coking property of nickel-based alumina catalysts. To investigate the anti-coking performance of the catalysts with spinel structure $NiAl_2O_4$, temperature programmed oxidation (TPO) was undertaken for two spent catalysts (NA-300 and NA-900) after catalytic reforming at 650 °C and 750 °C. The results are presented in Figure 7. Before the TPO experiment,

the samples were pretreated at 300°C under nitrogen atmosphere to ensure that the samples contained no crystal water. Therefore, the peaks on TPO curves in Figure 7 could only be caused by the oxidation of carbon deposit and nickel. One research [36] reported two kinds of carbon species on the catalyst surface of Ni/Al_2O_3, which are the amorphous type carbon and inert type carbon respectively. The amorphous carbon (or active carbon) can be oxidized below 300°C and the inert carbon (or coke) can be oxidized above 500°C. The nickel particles can be oxidized between 400°C and 450°C. Another research about the oxidation kinetics of small nickel particles [37] also proved that the small nickel particles could be oxidized between 300°C and 600°C. Based on these reports, we can identify the species on the catalyst surface by different oxygen consumption peaks on the TPO curves. There are three oxidation peaks on the TPO curves of the two spent catalysts. The first peak at a temperature below 200°C is the oxidation peak of amorphous carbon, the second peak at a temperature between 350°C and 500°C could be assigned to the oxidation of nickel particles, and the third one near 700°C corresponded to the oxidation of inert carbon on the catalyst surface. So both the amorphous and inert carbon species are loaded on the two spent catalysts. Generally, the amorphous carbon in the reforming process is easily oxidized by CO_2. However, excessive amorphous carbon will be converted into inert carbon with the reforming proceeding, thus leads to the catalyst deactivation. As can be seen from Figure 7, the amount of inert carbon on both two spent catalysts (NA-300 and NA-900) is very small, which is due to the fact that the two catalysts samples did not run for a long time. However, it's observed that more amorphous carbon deposited on the surface of catalyst NA-300 (without spinel structure) than NA-900 (including spinel structure), which provides abundant carbon source that is more easily converted to inert carbon and leads to catalyst deactivation. The catalyst with spinel structure $NiAl_2O_4$ possesses smaller nickel particle size, which leads to a better carbon elimination performance [28]. This is favorable for anti-coking. At the same time, comparing the

oxidation temperature of the amorphous carbon of the two spent catalysts, it can be found that the amorphous carbon species on the surface of the catalyst NA-900 (including spinel) has a higher oxidation temperature due to the developed microporous structure of the spinel structure, which results in a more compact combination of the deposited carbon and the catalyst. Combined with the previous catalyst characterization, it may be suggested that the main properties of the catalyst with spinel structure that affect the catalytic performance are pore size, microporous structure, small crystallite size, and the interaction between metal and support. These factors make the catalyst possess higher carbon deposition resistance and sintering resistance.

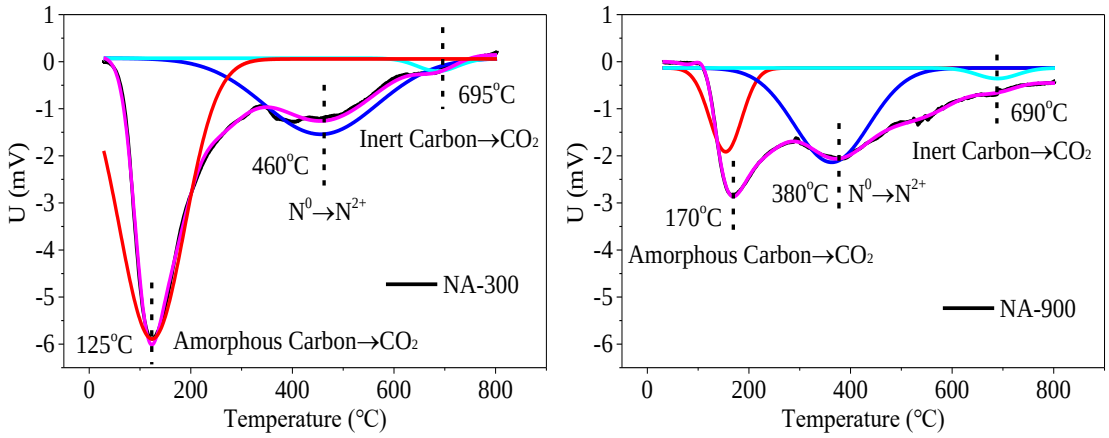

Figure 7 O_2-TPO of two spent catalysts (NA-300 and NA-900)

3.3 Biomass pyrolysis-reforming

The reforming of simulated pyrolysis gas (CH_4+CO_2) is just a main reaction in the biomass pyrolysis-reforming system. It is also necessary to apply the as-prepared catalysts to the actual reforming of gaseous products from rice husks pyrolysis to illustrate the catalytic performance. Therefore, the four nickel-based aluminum spinel catalysts were applied into pyrolysis-reforming of rice husks in relation to syngas production to fully demonstrate the performance of the catalyst with spinel structure. The four catalysts were reduced firstly. The detailed reduction conditions of four catalysts were the same as Table S2. The yield, mass balance,

and gas compositions of CO, H_2, CO_2, CH_4, and C_2-C_4 hydrocarbons during the pyrolysis-reforming of rice husks are presented in Table 3 and Figure 8.

As shown in Table 3 the char yield is stabilized around 37-38 wt. % since pyrolysis of the rice husks in the first stage reactor was the same for every experiment. The mass balance of the four groups of experiments was above 94%, which indicates the reliability of the results. As the calcination temperature increases, the spinel structure formed in the catalyst has a significant impact on the catalytic performance of the catalyst. The syngas yield was significantly increased for the catalyst with spinel (NA-900) compared with the catalyst without spinel (NA-300). The resulting spinel structure in catalyst also has a significant influence on the product gas composition. It can be observed from Figure 8 that the CO proportion gradually increases, H_2 proportion increases remarkably, and the O_2, CH_4, and C_2-C_4 hydrocarbons decrease continuously. Comparing the catalytic performance of two typical catalysts NA-300 and NA-900, it's found that the proportion of syngas in product gas of pyrolysis-reforming using NA-900 with spinel structure increases significantly. And the catalyst with spinel structure also shows the better catalytic performance of heavy hydrocarbon (C_2-C_4) than the common nickel-based alumina without spinel structure. But the proportion of CO_2 is maintained close to 24.5%. After the addition of steam, the main reaction in the system is occupied by steam reforming and the hydrocarbons from pyrolysis are preferentially reformed with steam.

Table 3 Mass balance from pyrolysis-reforming of biomass with four catalysts.

Catalyst bed	NA-300	NA-500	NA-700	NA-900
Char/wood (wt. %)	38	37	38	38
Syngas yield (mmol H_2 g^{-1} sample)	10.776	9.589	12.16	13.40
Volume ratio of H_2/CO	2.19	1.92	2.19	2.35
Mass balance (wt. %)	96.54	94.65	96.16	94.10

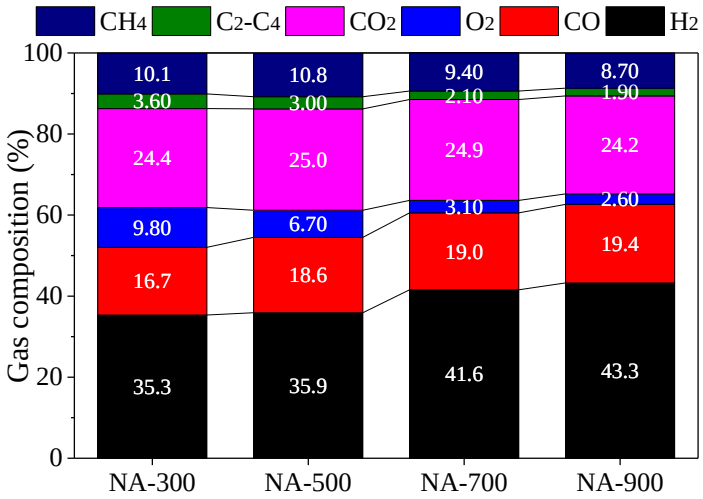

Figure 8 Gas composition from pyrolysis-reforming of biomass (Rice husk: 1 g, Catalyst dosage: 0.25 g, N_2 flow rate: 100 mL/min, Water: 4 mL/h, Pyrolysis temperature: 600 ℃, Reforming temperature: 800 ℃)

4. Conclusions

In this work, the relationship between textural properties of spinel in nickel-based alumina and the catalytic performance has been illustrated in two reaction systems of simulated pyrolysis gas (CH_4+CO_2) and real reforming of gaseous products from rice husks pyrolysis with four kinds of nickel-based alumina catalysts. It's indicated that the spinel structure could improve the catalytic performance and the anti-coking property of the catalysts. In the actual reforming of gaseous products from rice husks pyrolysis, the spinel structure catalysts showed better hydrocarbon conversion performance and higher syngas yield. Various characterization results combined with mechanism analysis proved that among various structural parameters, the spinel structure could improve the surface microporous properties and increase the pore size of the catalyst, which is closely related to the catalytic performance. When a spinel structure is formed in the catalyst, the nickel species will change the existing form, which also has a significant impact on the performance of the catalyst. Generally, the catalyst with spinel has a better catalytic performance and ability of anti-coking.

Supporting Information

A Word document containing Figure S1, Table S1 and Table S2.

Acknowledgment

This work was supported by the National Natural Science Foundation of China [grant number 51576048]; and Natural Science Foundation of Jiangsu Province [grant number BK20181142].

References

(1) Horlyck, J.; Lewis, S.; Amal, R.; Scott, J. The Impact of La Doping on Dry Reforming Ni-Based Catalysts Loaded on FSP-Alumina. *Top. Catal*. **2018**, *61(18-19)*, 1842-1855.

(2) Ma, Z.; Bai, J.; Bai, Z.; Kong, L.; Guo, Z.; Yan, J.; Li, W. Mineral Transformation in Char and Its Effect on Coal Char Gasification Reactivity at High Temperatures, Part 2: Char Gasification. *Energ. Fuel* **2014**, *28(3)*, 1846-1853.

(3) Kathiraser, Y.; Wang, Z.; Kawi, S. Oxidative CO_2 Reforming of Methane in $La_{0.6}Sr_{0.4}Co_{0.8}Ga_{0.2}O_{3-\delta}$ (LSCG) Hollow Fiber Membrane Reactor. *Environ. Sci. Technol.* **2013**, *47(24)*, 14510-14517.

(4) Chen, C.; Zhang, S.; Xu, K.; Luo, G.; Yao, H. Experimental and Modeling Study of Char Gasification with Mixtures of CO_2 and H_2O. *Energ. Fuel* **2016**, *30(3)*, 1628-1635.

(5) Pornmai, K.; Ngamkala, W.; Rirksomboon, T.; Ouraipryvan, P.; Chavadej, S. Reforming of CO_2-Containing Natural Gas with Steam and Partial Oxidation over Ni Catalysts in Corona Discharge for Synthesis Gas Production. *Ind. Eng. Chem. Res.* **2019**, *58(16)*, 6203-6217.

(6) Gil-Calvo, M.; Jiménez-González, C.; De-Rivas, B.; Gutiérrez-Ortiz, J. I.; López-Fonseca, R. Novel Nickel Aluminate-Derived Catalysts Supported on Ceria and Ceria-Zirconia for Partial Oxidation of Methane. *Ind. Eng. Chem. Res.* **2017**, *56(21)*, 6186-6197.

(7) Sadhwani, N.; Adhikari, S.; Eden, M. R. Biomass gasification using carbon dioxide: effect of temperature, CO_2/C ratio, and the study of reactions influencing the process. *Ind. Eng. Chem. Res.* **2016**, *55(10)*, 2883-2891.

(8) Dutta, P. P.; Das, A.; Pandey, V.; Devi, M. Fuel Characteristics of Some Locally Available Biomass as a Potential Gasification Feedstock for Thermal Application. *Ind. Eng. Chem. Res.* **2014**. *53(51)*, 19806-19813.

(9) Cao, J. P.; Liu, T. L.; Ren, J.; Zhao, X. Y.; Wu, Y.; Wang, J. X.; Ren, X. Y.; Wei, X. Y. Preparation and characterization of nickel loaded on resin char as tar reforming catalyst for biomass gasification. *J. Anal. Appl. Pyrol*. **2017**, *127*, 82-90.

(10) Song, M.; Jin, B.; Xiao, R.; Yang, L.; Wu, Y.; Zhong, Z.; Huang, Y. The comparison of two activation techniques to prepare activated carbon from corn cob. *Biomass Bioenerg*. **2013**, *48*, 250-256.

(11) Dong, L.; Wu, C.; Ling, H.; Shi, J.; Williams, P. T.; Huang, J. Development of Fe-Promoted Ni-Al Catalysts for Hydrogen Production from Gasification of Wood Sawdust. *Energ. Fuel* **2016**, *31(3)*, 2118-2127.

(12) Arregi, A.; Amutio, M.; Lopez, G.; Bilbao, J.; Olazar, M. Evaluation of thermochemical routes for hydrogen production from biomass: A review. *Energ. Convers. Manage*. **2018**, *165*, 696-719.

(13) Richardson, Y.; Blin, J.; Volle, G.; Motuzas, J.; Julbe, A. In situ generation of Ni metal nanoparticles as catalyst for H_2-rich syngas production from biomass gasification. *Appl. Catal. A-Gen.* **2010**, *382(2)*, 220-230.

(14) Sikarwar, V. S.; Zhao, M.; Clough, P.; Yao, J.; Zhong, X.; Memon, M. Z.; Shah, N.; Anthony, E. J.; Fennell, P. S. An overview of advances in biomass gasification. *Energ. Environ. Sci.* **2016**, *9(10)*, 2939-2977.

(15) Kumagai, S.; Alvarez, J.; Blanco, P. H.; Wu, C.; Yoshioka, T.; Olazar, M.; Williams, P. T. Novel Ni-Mg-Al-Ca catalyst for enhanced hydrogen production for the pyrolysis-gasification of a biomass/plastic mixture. *J. Anal. Appl. Pyrol.* **2015**, *113*, 15-21.

(16) Garcia, L.; Benedicto, A.; Romeo, E.; Salvador, M. L.; Arauzo, J.; Bilbao, R. Hydrogen Production by Steam Gasification of Biomass Using Ni-Al Coprecipitated Catalysts Promoted with Magnesium. *Energ. Fuel* **2002**, *16(5)*, 1222-1230.

(17) Jiang, L.; Liu, C.; Hu, S.; Wang, Y.; Xu, K.; Su, S.; Xiang, J. Catalytic behaviors of alkali metal salt involved in homogeneous volatile and heterogeneous char reforming in steam gasification of cellulose. *Energ. Convers. Manage*. **2018**, *158*, 147-155.

(18) Sahli, N.; Petit, C.; Roger, A. C.; Kiennemann, A.; Libs, S.; Bettahar, M. M. Ni catalysts from $NiAl_2O_4$ spinel for CO_2 reforming of methane *Catal. Today* **2006**, *113(3-4)*, 187-193.

(19) Zhou, L.; Li, L.; Wei, N.; Li, J.; Basset, J. M. Effect of $NiAl_2O_4$ Formation on Ni/Al_2O_3 Stability during Dry Reforming of Methane. *ChemCatChem*. **2015**, *7(16)*, 2508-2516.

(20) Benrabaa, R.; Barama, A.; Boukhlouf, H.; Guerrero-Caballero, J.; Rubbens, A.; Bordes-Richard, E.; Löfberg, A.; Vannier, R. N. Physico-chemical properties and syngas production via dry reforming of methane over $NiAl_2O_4$ catalyst. *Int. J. Hydrogen Energ.* **2017**, *42(18)*, 12989-12996.

(21) Jiménez-González, C.; Boukha, Z.; De-Rivas, B.; González-Velasco, J. R.; Gutiérrez-Ortiz, J. I.; López-Fonseca, R. Behavior of Coprecipitated $NiAl_2O_4/Al_2O_3$ Catalysts for Low-Temperature Methane Steam Reforming. *Energ. Fuel* **2014**, *28(11)*, 7109-7121.

(22) Jiménez-González, C.; Gil-Calvo, M.; De-Rivas, B.; González-Velasco, J. R.; Gutiérrez-Ortiz, J. I.; López-Fonseca, R. Oxidative Steam Reforming and Steam Reforming of Methane, Isooctane, and N-

Tetradecane over an Alumina Supported Spinel-Derived Nickel Catalyst. *Ind. Eng. Chem. Res.* **2016**, *55(14)*, 3920-3929.

(23) Chen, F.; Wu, C.; Dong, L.; Vassallo, A.; Williams, P. T.; Huang, Characteristics and catalytic properties of Ni/$CaAlO_X$ catalyst for hydrogen-enriched syngas production from pyrolysis-steam reforming of biomass sawdust. *Appl. Catal. B-Environ.* **2016**, *183*, 168-175.

(24) Yu, L.; Song, M.; Gao, R.; Wei, Y. Preparation and application of nickel based carbon fibers for the steam reforming of methane. *React. Kinet. Mech. Cat.* **2017**, *120(2)*, 477-488.

(25) Wei, Y.; Song, M.; Yu, L.; Gao, R.; Meng, F.; Xiao, J.; Zhang, Y. Promotion Effect of SiO_2 on the Catalytic Performance of Ni/CF for Biomass Derived Gas Reforming. *Ind. Eng. Chem. Res.* **2018**, *57(32)*, 10851-10858.

(26) Dong, L.; Wu, C.; Ling, H.; Shi, J.; Williams, P. T.; Huang, J. Promoting hydrogen production and minimizing catalyst deactivation from the pyrolysis-catalytic steam reforming of biomass on nanosized $NiZnAlO_X$ catalysts. *Fuel* **2017**, *188*, 610-620.

(27) Tao, F. F.; Shan, J. J.; Nguyen, L.; Wang, Z.; Zhang, S.; Zhang, L.; Wu, Z.; Huang, W.; Zeng, S.; Hu, P. Understanding complete oxidation of methane on spinel oxides at a molecular level. *Nat. Commun*. **2015**, *6*, 7798.

(28) Christensen, K. O.; Chen, D.; Lødeng. R.; Holmen, A. Effect of supports and Ni crystal size on carbon formation and sintering during steam methane reforming. *Appl. Catal. A-Gen.* **2006**, *314(1)*, 9-22.

(29) Meng, F.; Song, M.; Wei, Y.; Wang, Y. The contribution of oxygen-containing functional groups to the gas-phase adsorption of volatile organic compounds with different polarities onto lignin-derived activated carbon fibers. *Environ. Sci. Pollut. Res.* **2019**, *26(7)*, 7195-7204.

(30) Song, M.; Zhang, W.; Chen, Y.; Luo, J.; Crittenden, J. C. The preparation and performance of lignin-based activated carbon fiber adsorbents for treating gaseous streams. Front. Chem. Sci. Eng. **2017**, 11(3), 328-337.

(31) Cai, W.; Yu, J.; Anand, C.; Vinu, A.; Jaroniec, M. Facile Synthesis of Ordered Mesoporous Alumina and Alumina-Supported Metal Oxides with Tailored Adsorption and Framework Properties. *Chem. Mater.* **2011**, *23(5)*, 1147-1157.

(32) Gangwar, J.; Gupta, B. K.; Tripathi, S. K.; Srivastava, A. K. Phase dependent thermal and spectroscopic responses of Al_2O_3 nanostructures with different morphogenesis. *Nanoscale* **2015**, *7(32)*, 13313-13344.

(33) Diebold, U.; Li, S. C.; Schmid, M. Oxide Surface Science. *Annu. Rev. Phys. Chem.* **2010**, *61*, 129-148.

(34) Fan, M. S.; Abdullah, A. Z.; Bhatia, S. Catalytic Technology for Carbon Dioxide Reforming of Methane to Synthesis Gas. *ChemCatChem.* **2009**, *1(2)*, 192-208.

(35) Serrano-Lotina, A.; Daza, L. Influence of the operating parameters over dry reforming of methane to syngas. *Int. J. Hydrogen Energ*. **2014**, *39(8)*, 4089-4094.

(36) Koo, K. Y.; Roh, H. S.; Seo, Y. T.; Seo, D. J.; Yoon, W. L.; Park, S. B. Coke study on MgO-promoted Ni/Al_2O_3 catalyst in combined H_2O and CO_2 reforming of methane for gas to liquid (GTL) process *Appl. Catal. A-Gen.* **2008**, *340(2)*, 183-190.

(37) Karmhag, R.; Niklasson, G. A.; Nygren, M. Oxidation kinetics of small nickel particles. *J. Appl. Phys.* **1999**, *85(2)*, 1186-1191.

Table of Contents (TOC) Graphic